

# Gold supported on well-ordered ceria films: nucleation, growth and morphology in CO oxidation reaction

J.-L. Lu,<sup>a,b</sup> H.-J. Gao,<sup>b</sup> S. Shaikhutdinov,<sup>a,\*</sup> and H.-J. Freund<sup>a</sup>

<sup>a</sup>Department of Chemical Physics, Fritz Haber Institute of the Max Planck Society, Faradayweg 4-6, 14195 Berlin, Germany

<sup>b</sup>Beijing National Laboratory for Condensed Matter Physics, Institute of Physics, Chinese Academy of Sciences, PO Box 603, Beijing 100080, China

Received 5 December 2006; accepted 4 January 2007

Structure of gold nanoparticles formed by physical vapor deposition onto thin ceria films was studied by scanning tunneling microscopy (STM). Gold preferentially nucleates on point defects present on the terraces of the well-ordered, fully oxidized films to a low density. The nucleation expands to the terrace step edges, providing a large variety of low-coordinated sites. Only at high coverage, the Au particles grow homogeneously on the oxygen-terminated CeO<sub>2</sub>(111) terraces. The morphology of Au particles was further examined by STM *in situ* and *ex situ* at elevated (up to 20 mbar) pressures of O<sub>2</sub>, CO, and CO + O<sub>2</sub> at 300 K. The particles are found to be stable in O<sub>2</sub> ambient up to 10 mbar, meanwhile gold sintering emerges at CO pressures above ~1 mbar. Sintering of the Au particles, which mainly proceeds along the step edges of the CeO<sub>2</sub>(111) support, is observed in CO + O<sub>2</sub> (1:1) mixture at much lower pressure (~10<sup>-3</sup> mbar), thus indicating that the structural stability of the Au/ceria catalysts is intimately connected with its reactivity in the CO oxidation reaction.

**KEY WORDS:** gold; ceria; CO oxidation; thin films; scanning tunneling microscopy.

## 1. Introduction

In the last decade, chemistry of gold has received much attention owing to unique catalytic properties observed for supported gold nanoparticles in many catalytic reactions such as low temperature CO oxidation, selective oxidation of propene to propene oxide, water gas shift reaction, NO reduction, selective hydrogenation of acetylene and butadiene, etc. (see recent review [1]). The nature of the active species in highly dispersed Au catalysts (ionic versus metallic, low-coordinated surface atoms versus metal/support interface) is a matter of extensive debates. Among many gold catalysts reported in the literature, those supported on the cerium oxide (CeO<sub>2</sub>) often show a superior activity ([2–9], and references therein). It should be mentioned that the reaction mechanisms, involving cationic Au<sup>3+</sup> and Au<sup>+</sup> species as the most active, have been reinforced after experimental observations by Flutzani-Staphanopolus and co-workers on the Au/CeO<sub>2</sub> catalysts [10]. Furthermore, Carrettin *et al.* [5] found that using nanocrystalline ceria as a support increases the activity of gold in CO oxidation by two orders of magnitude as compared to a “conventional” ceria support. This effect was assigned to the presence of significant amounts of cationic gold species in these samples [5,6].

In order to establish structure–reactivity relationships for the Au/ceria systems on a molecular level, we suggest a use of the model systems whereby gold particles are formed by physical vapor deposition onto well-ordered ceria films grown on a metal single crystal substrate. This approach has been proven to be efficient for many other metal/oxide systems (see reviews [11–14]). The planar model catalysts allow one to precisely control the structure of the systems and investigate the processes occurring on the catalyst surface by employing various surface sensitive techniques. Recent fundamental studies on gold surfaces have been reviewed by Meyer *et al.* [15].

For relatively inert surfaces like of gold, a so called “pressure gap” between model studies under vacuum and realistic conditions may be very crucial. Even though the number of publications on gold catalysts increases tremendously, structural *in situ* studies under realistic conditions are still rare. For example, Gates and co-workers use X-ray absorption techniques (XANES, EXAFS) and infrared spectroscopy to monitor the oxidation states of Au in CO oxidation and ethylene hydrogenation reactions over Au/MgO [16]. A similar approach has been recently used by Kung and co-workers [17] for studies of the CO oxidation reaction over Au/TiO<sub>2</sub>, by Wang *et al.* [18] on Au/CeO<sub>2</sub> catalysts for water gas-shift reaction, Overbury *et al.* [19] on Au/TiO<sub>2</sub> catalysts of CO oxidation and Wieher *et al.* [20] of different gold catalysts. A recent paper by Hutchings

\*To whom correspondence should be addressed.  
E-mail: shamil@fhi-berlin.mpg.de

*et al.* [21] reports on complementary studies performed in different groups on the same Au/Fe<sub>2</sub>O<sub>3</sub> catalysts, in particular showing good potentials for using Au<sup>197</sup> Mössbauer spectroscopy to elucidate the role of cationic species in reactions.

In this respect, one of the important issues relates to possible structural modifications of the gold catalyst in a reactive environment. Interaction with the reactive gas may cause a weakening of the Au–Au bonds within the particle and as a result to a disruption of the structure of the particle. Also, the strength of interaction between the gold particle and the support may play a significant role in determining the stability of these systems at higher pressures.

For example, Valden *et al.* [22] observed by scanning tunneling microscopy (STM) *ex situ* a form of Ostwald ripening (the growth of large particles at the expense of small particles) by exposing the Au/TiO<sub>2</sub>(110) surface to 10 Torr of O<sub>2</sub> for 2 h at room temperature. This effect was found to be stronger in a CO + O<sub>2</sub> (2:1) mixture. Kolmakov and Goodman [23] further studied the sintering behavior of Au/TiO<sub>2</sub>(110) under CO oxidation conditions with *in situ* STM. The Au particles were found to undergo severe Ostwald ripening at 720 Pa and 450 K. The authors suggested that the presence of oxygen served to weaken Au–Au bonds, thereby promoting sintering. This work also highlighted the importance of considering tip-induced effects during high-pressure STM studies, including cluster movement by or adhesion to the tip, and also possible gas-induced changes in the tunneling process.

Recently, Starr *et al.* [24] studied the morphology of Au particles deposited on thin FeO(111) films at elevated pressures of CO, O<sub>2</sub>, CO + O<sub>2</sub>, and H<sub>2</sub> using *in situ* STM at room temperature. The Au particles were quite stable in oxygen and hydrogen environments at pressures up to 2 mbar. However, in CO and CO + O<sub>2</sub> atmospheres, the destabilization of Au particles located at the step edges was observed at  $\sim 10^{-3}$  mbar leading to the formation of mobile Au species, which migrated across the oxide surface. The results were rationalized on the basis of a stronger interaction of gold with CO, as compared to O<sub>2</sub> and H<sub>2</sub>, which significantly weakens the Au/support interaction for the smallest particles. In addition, the authors highlighted the effects of ambient gas impurities, which may lead to erroneous conclusions about morphological changes of the gold surfaces at elevated pressures.

In this work, we report on structural characterization of Au/ceria model catalysts, particularly on nucleation and growth of gold deposited on the well ordered ceria films. The morphology of the gold nanoparticles was further examined *in situ* in CO, O<sub>2</sub>, and CO + O<sub>2</sub> ambient by STM. The results obtained aid in our understanding of the structure–reactivity relationships for the ceria supported gold catalysts, in

particular its structural stability under the reaction conditions.

## 2. Experimental

The experiments were performed in an ultra-high vacuum (UHV) chamber (base pressure  $2 \times 10^{-10}$  mbar) equipped with a STM (Omicron), a four-grid optics for Auger electron spectroscopy and low energy electron diffraction (AES/LEED, Specs), and standard facilities for surface cleaning.

The Ru(0001) single crystal (10 mm diameter and 2 mm thick, Mateck) was clamped to a Mo holder and heated from the backside of the crystal using electron bombardment from a W filament. The temperature was controlled using a type K thermocouple spot-welded to the edge of the crystal and a feedback system (Schlichting Phys. Instrum). The clean surface was prepared using cycles of Ar<sup>+</sup> sputtering followed by annealing in UHV to 1300 K.

The preparation recipe for the ceria films grown on a Ru(0001) substrate has been adopted from the one suggested by Mullins *et al.* [25] and modified in order to form wide atomically flat terraces. Briefly, approximately 6 monolayers (ML) of ceria was deposited onto the clean Ru(0001) surface at the rate of 0.2 ML/min in  $1 \times 10^{-7}$  mbar of O<sub>2</sub> at 790 K followed by annealing at 980 K in  $4 \times 10^{-7}$  mbar of O<sub>2</sub>. Oxygen was pumped out after sample cooling down to 400 K. Cerium was evaporated from a W crucible heated using ceramic protected W wires wrapped around the crucible. For each Au/sample used in the “high pressure” experiments, a new ceria film was prepared.

Gold (99.99%, Goodfellow) was deposited onto the ceria films from a W crucible at a rate of  $\sim 0.05$  ML/min using an electron beam assisted evaporator (Focus, EFM3). During evaporation the sample was biased at the same potential as the Au source in order to prevent accelerating of the metal ions towards the sample.

The STM is housed in a small chamber separated from the main chamber by a gate valve to allow *in situ* STM measurements in different gas ambient. The gas pressure in STM chamber was measured using a cold-cathode and MKS Baratron dual gauge system with overlapping pressure ranges. An additional, Au-plated high-pressure cell is attached to the main chamber allowing treatments similar to those in the STM chamber for *ex situ* measurements. Combining the *ex situ* and *in situ* measurements allows one to ascertain whether observed morphological changes are potentially induced by STM tip modifications at elevated pressure at least in the case of irreversible changes. Commercial Pt/Ir tips (L.O.T.-Oriol GmbH) were used.

Great care was taken to ensure the cleanliness of gases used (CO and O<sub>2</sub> (both 5.0, AGA Gas)) through repeated rinsing of the gas handling system and the

STM chamber prior to use. In addition, the gas from the stainless bottle was introduced through a cold trap kept at liquid nitrogen for CO, and  $\sim 200$  K for O<sub>2</sub> and CO + O<sub>2</sub> mixture.

### 3. Results and discussion

#### 3.1. Nucleation and growth

The morphology of the CeO<sub>2</sub>(111) films has been examined by STM prior to gold deposition. As previously shown [26], the clean films basically expose flat terraces, which often consist of several domains. The terraces are mostly circular in shape that suggests that the steps may expose a variety of the undercoordinated atoms located on edges, which in turn may act as nucleation centers for the gold particles. Indeed, figure 1a demonstrates that interaction of gold with the step edges is much stronger than with the regular terrace, which is oxygen terminated CeO<sub>2</sub>(111) surface in nature [25]. Only a few Au particles are observed on the terraces at this coverage, which can be associated with the point defects present on the terraces. (Henceforth we will refer to “point defects” as the defects, which include vacancies and their agglomerates like dimer, trimers, etc. previously observed by STM on the CeO<sub>2</sub>(111) surface [26–30]). Note also, that this film was not inspected by LEED or AES before Au deposition, which may cause electron beam damaging effects.

Due to a low density of the point defects on this sample, it is difficult to judge whether Au preferentially nucleates on the point defects or the step edges. In order to increase the number of defects in our ceria films, we have lowered the oxygen pressure during preparation from  $4 \times 10^{-7}$  to  $4 \times 10^{-8}$  mbar, which according to Mullins *et al.* [25] partially reduces the ceria surface. Figure 1b shows that, about 20% of all particles are located on the terraces of the reduced sample at the

same total amounts of gold as used for the fully oxidized sample shown in figure 1a. Therefore, we can conclude that partial reduction of the ceria increases the number of the point defects, which strongly interact with the deposited gold.

Figure 2 presents a series of STM images of gold deposited onto partially reduced ceria films at room temperature. At the lowest Au coverage studied, the Au particles are mostly found on the terraces as shown in figure 2a. Increasing gold coverage results in the higher number of the particles at the step edges (see figure 2b). Only after apparent saturation of the nucleation sites on steps, the particles grow randomly over the whole surface (figure 2c). These results suggest that gold first nucleates on the point defects and then on the step edges. In other words, gold interacts with the point defects more strongly than with undercoordinated sites on the step edges.

Further increasing gold coverage basically increases the particle size at nearly constant particle density as shown in figure 2d, e and two diagrams below, which summarize the data on the particle size and density as a function of gold coverage. The aspect ratio (height to diameter) measured ( $\sim 0.3$ ) suggests that the particles are hemispherical (taking into account a well known tip deconvolution effect). The aspect ratio is found to be rather independent on the gold coverage, thus indicating a three-dimensional growth mode from the onset, which can be easily explained by a large lattice mismatch between gold and ceria ( $\sim 30\%$ ). It seems plausible that it is the large mismatch that inhibits Au particles from further growing and favors the formation of new particles on the terraces upon increasing coverage as observed in figure 2.

In addition, the inset in figure 2e shows that the Au particles are well faceted with the top facet exhibiting a hexagonal shape. These facets likely expose the Au(111) surface according to electron microscopy studies of

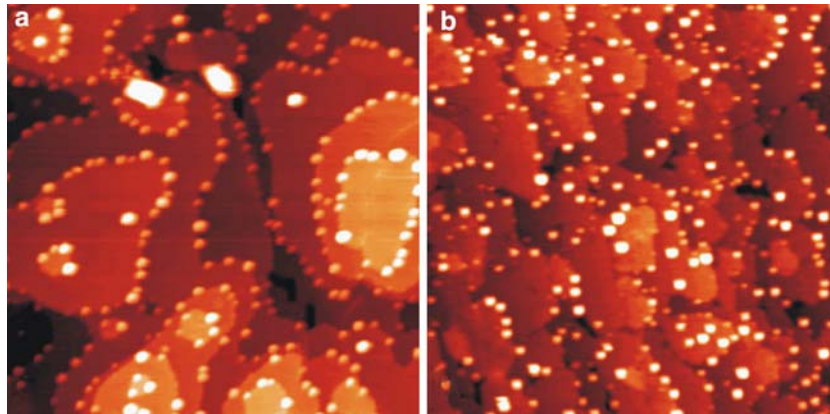


Figure 1. STM images of 0.1 ML of gold deposited at 300 K on the fully oxidized (a) and partially reduced (b) CeO<sub>2</sub>(111) films. The reduced film was prepared by the oxidation at  $4 \times 10^{-8}$  mbar pressures which an order of magnitude lower than used for fully oxidized film ( $4 \times 10^{-7}$  mbar). Image size is  $150 \times 150$  nm<sup>2</sup>; tunneling parameters are  $V_s = 4.1$  V,  $I = 0.1$  nA (a);  $V_s = 4.6$  V,  $I = 0.06$  nA (b).



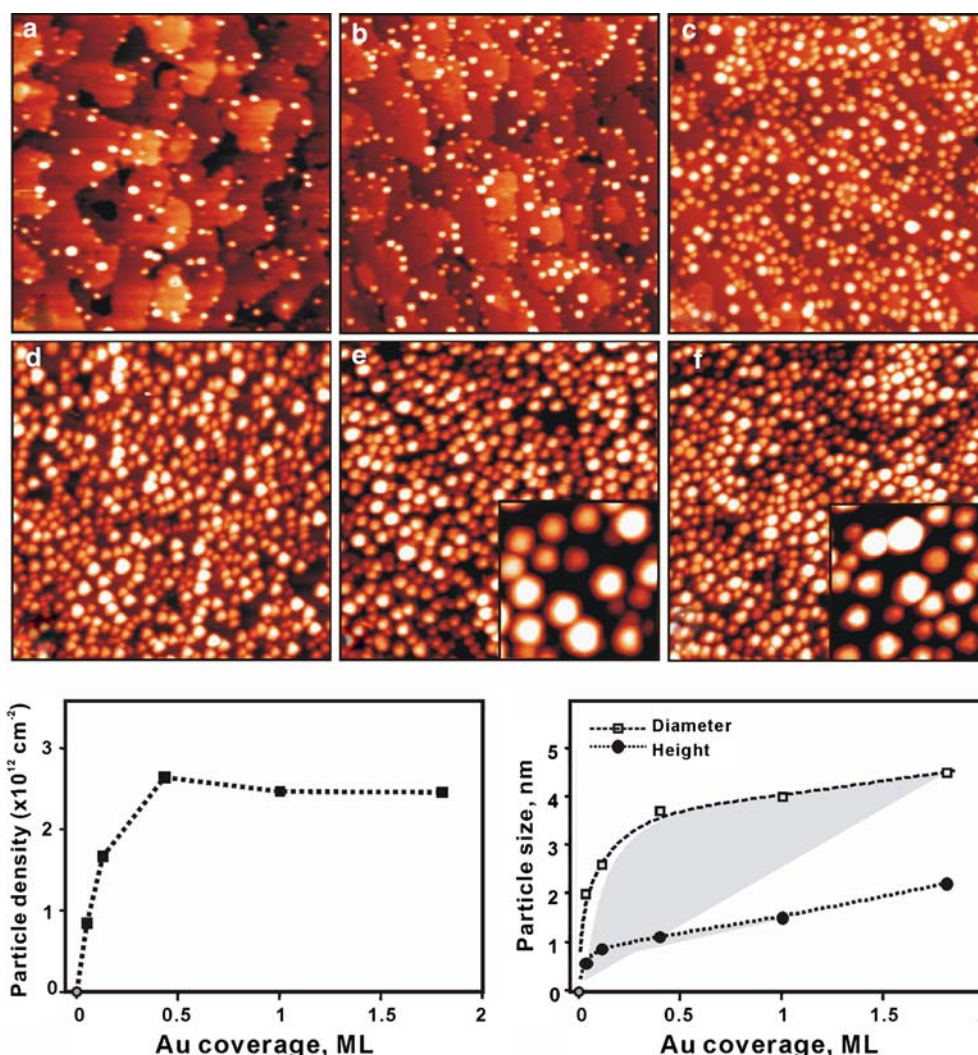


Figure 2. STM images of Au particles deposited on the partially reduced ceria films to a coverage 0.05 (a), 0.15 (b), 0.4 (c), 1 (d) and 2 ML (e). Shown in (f) is the sample (e) after annealing to 500 K in UHV. The tunneling parameters are  $V_s = 4.5$  V and  $I = 0.1$  nA for all images. Image size:  $150 \times 150$  nm<sup>2</sup> and  $30 \times 30$  nm<sup>2</sup> (insets). The diagrams show particle density (left) and apparent size (right) as a function of gold coverage.

Akita *et al.* [31] where an epitaxial relationship between (111) planes of Au and CeO<sub>2</sub> has been observed for hemispherical Au particles on the powdered Au/ceria catalysts. Figure 2f shows that annealing of the samples to 500 K in UHV did not result in any sintering even for the highly loaded Au/ceria sample, thus indicating a good thermal stability of the system towards sintering in vacuum.

### 3.2. Morphology in a reaction atmosphere

Figure 3 shows a few snapshots from the “STM movie” recorded on the Au/ceria sample while introducing CO + O<sub>2</sub> (1:1) mixture into the STM chamber. No discernable changes were found unless the pressure reached  $\sim 10^{-3}$  mbar. As seen from figure 3b, c, the ceria surface between the Au particles became rougher as compared to the flat terraces imaged in UHV (figure 3a).

In addition, small features (<1 nm in size) emerge on the terraces as shown in the inset in figure 3c.

The regions (A) and (B) in figure 3a indicate groups of the Au particles where the morphological changes have been most clearly observed. Comparing the images (b–f) recorded at nearly the same gas pressure ( $\sim 10^{-3}$  mbar), one can see that some particles in the region (A) gradually vanish and are almost disappeared in the image (f). Meanwhile, the groups (B) exhibit a form of Ostwald ripening, which results in the formation of larger particles at the expense of neighboring small particles. Although the image resolution can slightly be affected by the presence of the ambient gas, the use of the size ratios for these particles clearly manifests the effect. It is also likely that the sintering process occurs through species migrating along the steps, as the changes are observed only for the particles in the close proximity.

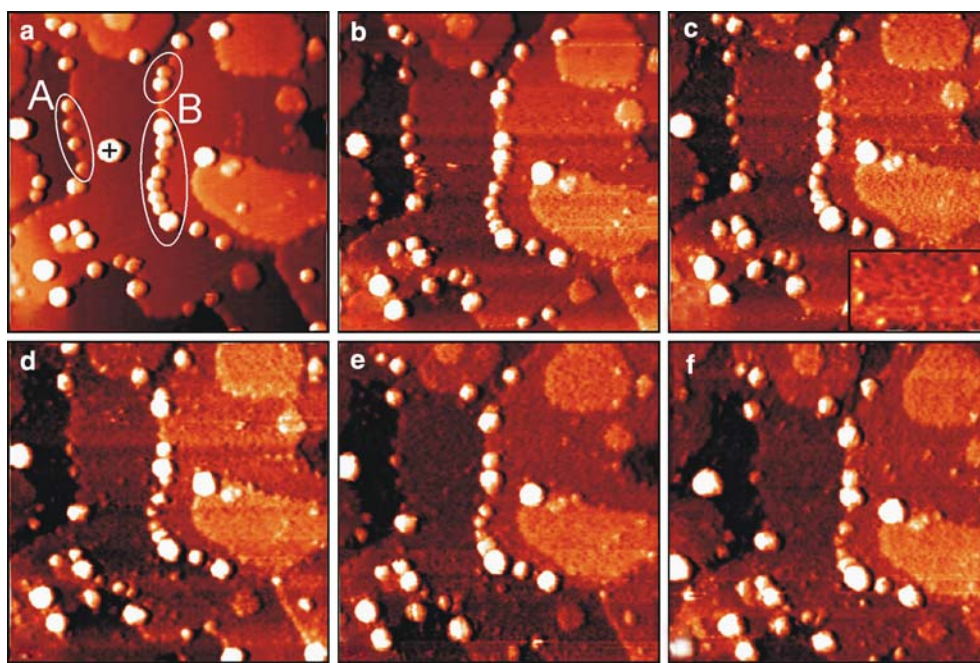


Figure 3. A series of snapshots from *in situ* "STM movie" from the 0.1 ML Au on fully oxidized ceria film while exposing to CO + O<sub>2</sub> (1:1) at 300 K at pressures  $< 10^{-8}$ ,  $5 \times 10^{-4}$ ,  $1 \times 10^{-3}$ ,  $1.2 \times 10^{-3}$ ,  $1.3 \times 10^{-3}$ , and  $2 \times 10^{-3}$  mbar for the images (a–f), respectively. Image size is  $75 \times 75$  nm<sup>2</sup>, and  $19 \times 11$  nm<sup>2</sup> for the inset in (c). Tunneling parameters:  $V_s = 4.0$  V,  $I = 0.1$  nA. The large particle marked by cross in (a) is removed by the tip while scanning. Regions (A) and (B) show two groups of the particles, where the reaction induced changes are the most clearly seen (see the text).

The sintering of the Au particles proceeds more efficiently at higher pressures. Figure 4 shows two large-scale STM images of the Au/ceria samples before (a) and after (b) exposing to 20 mbar of CO + O<sub>2</sub> (1:1) for 60 min, both recorded in UHV. The comparison of the corresponding particles size distributions clearly show that, after the reaction, the Au particles became larger, on average, and exhibit a much broader distribution as compared to the pristine samples. In addition, the ceria surface between the particles became highly corrugated (as it is observed *in situ* in figure 3), indicating that this roughening is caused by the surface reactions and not by the gas/tip interaction. However, the origin of the small features observed on the ceria terraces is not straightforward. In contrast to the FeO support previously studied in our group, which is essentially inert towards CO and O<sub>2</sub>, the ceria surface may react with these molecules [34,35]. Therefore, overall roughening of the ceria surface cannot be unambiguously assigned to the formation of Au clusters diffusing across the terraces as it was suggested for the Au/FeO system [24]. Figure 5 shows that annealing in vacuum to 700 K can apparently remove most of these small species such that well-isolated small particles are formed, which are  $\sim 2$  nm in lateral size and 0.3 nm in height. However, the chemical composition of these monolayer islands remains unknown (AES analysis of this surface did not reveal new elements in a definitive manner).

For comparison, we have also performed similar experiments in pure CO and O<sub>2</sub> ambient. Figure 6

shows *in situ* STM images of the same area at  $< 10^{-8}$ ,  $5 \times 10^{-4}$ , 0.1, 1.4, 5.4, and 7.4 mbar of CO, respectively. Here, we have to recall that imaging of gold nanoparticles is known to often accompany by the tip-induced motion of the particles as well as by adhesion (and depositing) particles to (from) the STM tip. Marked by the triangle in figure 6 is the region where one of the particles is moved by the tip (compare (a) and (b)) and then two particles apparently disappeared (compare (b) and (c)). A similar effect is observed in the region indicated by the oval: two  $\sim 3$  nm particles disappear without significant growth of the neighboring particles. Finally, indicated by the cross in figure 6c is the large particle (presumably Au), which is dropped from the tip, resulting also in partial lowering of the image resolution. Therefore, we have assigned these effects to be induced by the tip rather than by CO ambient. Bearing all this in mind while analyzing the STM images we have concluded that the Au particles are fairly stable in CO ambient, although some particles were found to gradually disappear while increasing the CO pressure above 1 mbar as indicated by the circles in figure 6d–f.

More significant morphological changes were observed after exposure to 20 mbar of CO for 60 min as shown in figure 7. A histogram analysis revealed that particle size distribution became broader, although the mean particle size is not significantly changed. Overall, the results show that gold sintering may occur in CO ambient at pressures above 1 mbar, at least.



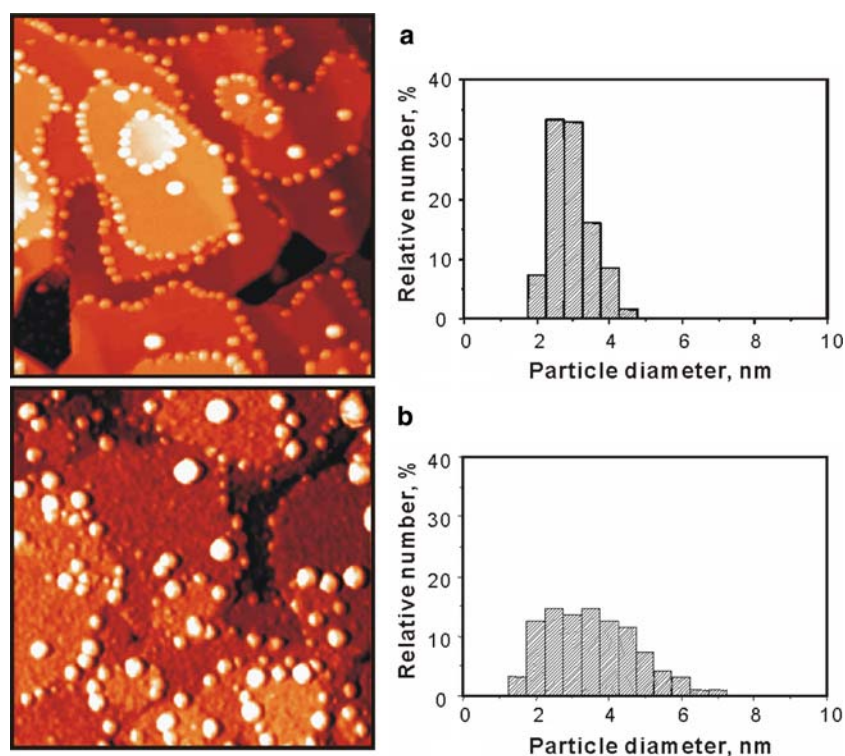


Figure 4. STM images of 0.1 ML Au on the  $\text{CeO}_2(111)$  film as prepared (a), and after exposure to 20 mbar of  $\text{CO} + \text{O}_2$  (1:1) for 60 min at 300 K (b). Image size is  $120 \times 120 \text{ nm}^2$ , tunneling parameters:  $V_s = 4.1 \text{ V}$ ,  $I = 0.1 \text{ nA}$  (a);  $V_s = 4.3 \text{ V}$ ,  $I = 0.1 \text{ nA}$  (b). The histograms show particle size distributions of the corresponding STM images.

Concerning the pure  $\text{O}_2$  environment, figure 8 shows two STM images of the Au/ceria sample before (a) and after (b) exposure to  $\sim 10$  mbar of  $\text{O}_2$  for 120 min at 300 K. No discernable changes were found after this treatment, which implies that the gold on ceria is more stable in an  $\text{O}_2$  environment than in  $\text{CO}$  and  $\text{CO} + \text{O}_2$ . On the one hand, this behavior is similar to that observed on  $\text{Au/FeO}(111)$ , where changes were not found in  $\text{O}_2$  (and  $\text{H}_2$ ) but in  $\text{CO}$  and  $\text{CO} + \text{O}_2$  ambient [24]. On the other hand, it is opposite to the behavior reported for the  $\text{Au/TiO}_2(110)$  system [22,23], where Ostwald ripening was observed in pure  $\text{O}_2$  and even

more severe in  $\text{CO} + \text{O}_2$  atmosphere but not in pure  $\text{CO}$ . These results suggest that structural stability strongly depends on the nature of the oxide support used.

For the  $\text{FeO}$  thin film, it seems plausible that all environmental effects are to be associated with the reactivity of gold only. As it is known, interaction of gold with  $\text{CO}$  is much stronger than with molecular  $\text{O}_2$  and  $\text{H}_2$  [24], therefore the effects of high pressures is observed only in the presence of  $\text{CO}$ . Meanwhile, titania and ceria belong to the class of the reducible oxides and can be directly involved in the interaction with  $\text{CO}$  and

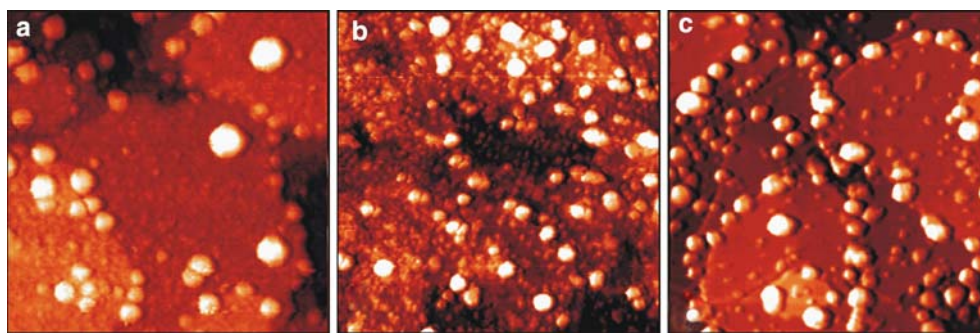


Figure 5. (a) STM image of the 0.1 ML Au on the  $\text{CeO}_2(111)$  film exposed to 20 mbar of  $\text{CO} + \text{O}_2$  (1:1) at 300 K and recorded in vacuum (a) and after subsequent annealing to 500 (b) and 700 K (c) in vacuum. Formation of the small features on the ceria surface between the gold particles are seen. Image size is  $80 \times 80 \text{ nm}^2$ , tunneling parameters are  $V_s = 4.1 \text{ V}$  and  $I = 0.1 \text{ nA}$ .

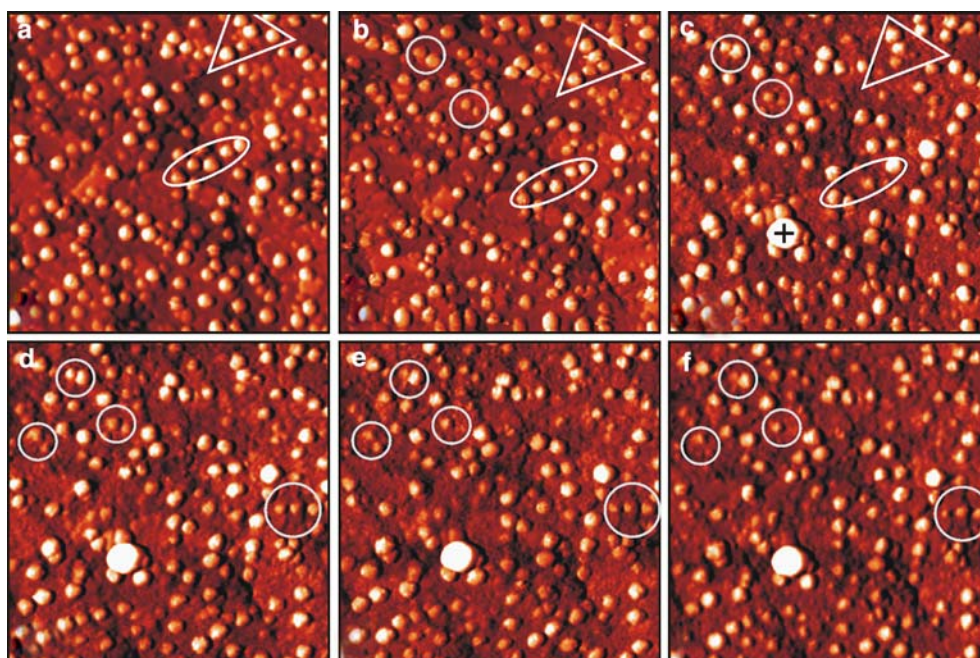


Figure 6. Six snapshots from the “STM movie” on 0.2 ML Au on the  $\text{CeO}_2(111)$  film with increasing CO pressure. The pressure is  $10^{-8}$ ,  $5 \times 10^{-4}$ , 0.1, 1.4, 5.4, and 7.4 mbar for images (a–f), respectively. Marked by the triangle and oval are two regions where tip induced effects were observed, while the circles indicate the particles, which gradually vanished upon increasing CO pressure. Image size is  $80 \times 80 \text{ nm}^2$ , tunneling parameters are  $V_s = 4.0 \text{ V}$ ,  $I = 0.08 \text{ nA}$ .

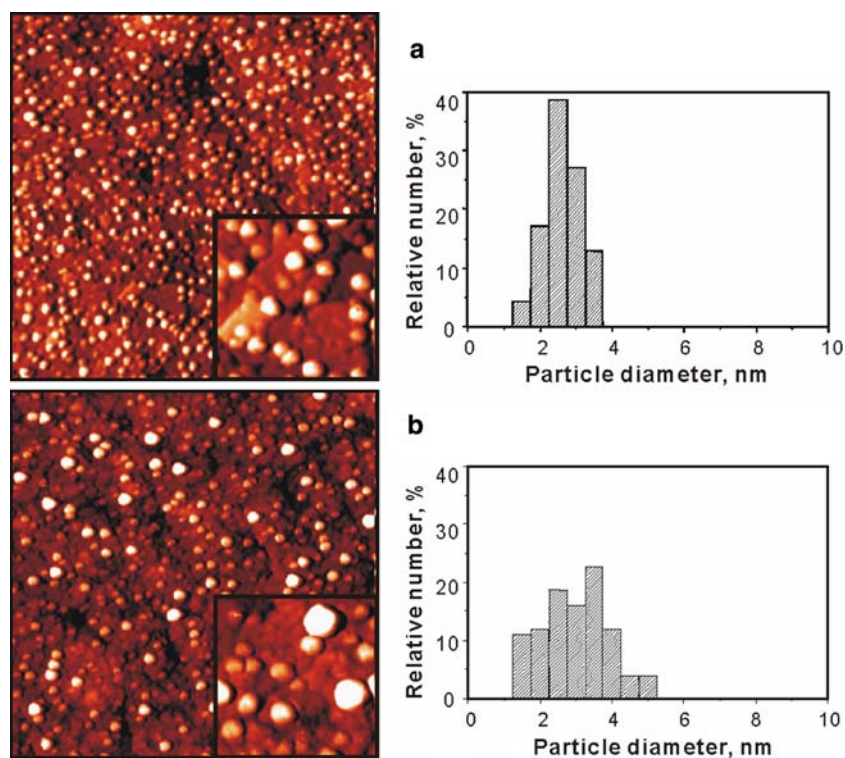


Figure 7. STM images of 0.2 ML Au on  $\text{CeO}_2(111)$  film as prepared (a), and after exposure to 20 mbar of CO for 60 min at 300 K (b). Image size is  $150 \times 150 \text{ nm}^2$ ,  $30 \times 30 \text{ nm}^2$  (for the insets), tunneling parameters are  $V_s = 3.7 \text{ V}$ ,  $I = 0.08 \text{ nA}$  (a);  $V_s = 3.7 \text{ V}$ ,  $I = 0.08 \text{ nA}$  (b). The histograms show the particle size distribution.



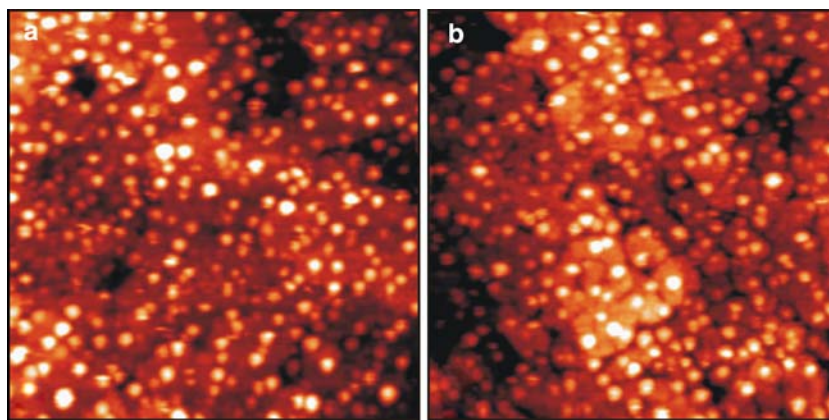


Figure 8. STM images of 0.2 ML Au on CeO<sub>2</sub>(111) film as prepared (a), and after exposure to 10 mbar of O<sub>2</sub> for 120 min at 300 K (b). Image size is 100 × 100 nm<sup>2</sup>, tunneling parameters are  $V_s = 4$  V,  $I = 0.1$  nA.

O<sub>2</sub> [32]. Therefore, the differences in the responses to the gas exposure for Au/TiO<sub>2</sub>(110) and Au/CeO<sub>2</sub>(111) systems can be linked to the different reactivity of the oxide supports themselves. In particular, the structure of the interface at the Au/oxide perimeter may play a role in the stability of the Au particles under reaction conditions. Both Au/ceria and Au/titania systems showed that gold sintering occurs much more efficiently under CO oxidation reaction conditions as compared to individual CO and O<sub>2</sub> gas exposures, which implies that the structural stability of the oxide supported Au catalysts is intimately connected with its reactivity.

#### 4. Summary

The structure of Au nanoparticles vapor-deposited on the CeO<sub>2</sub>(111) films has been studied by STM. Gold preferentially nucleates at point defects present on the terraces with a low density on the well-ordered, fully oxidized films. At increasing gold coverage, particles nucleate at the step edges, which provide a large variety of low-coordinated sites. Only at high coverage, the Au particles grow homogeneously on the flat CeO<sub>2</sub>(111) terraces. The results suggest that gold exhibits a three-dimensional growth mode from the onset and it forms the nanoparticles, which are fairly stable towards sintering in vacuum.

The morphology of the supported Au particles have been further studied by *in situ* and *ex situ* STM in CO, O<sub>2</sub> and CO + O<sub>2</sub> environment at room temperature. No visible changes are observed after exposing Au particles to pure O<sub>2</sub> up to ~10 mbar. In the pure CO ambient, a form of Ostwald ripening emerges above ~1 mbar. Meanwhile, sintering of the Au particles is observed in CO + O<sub>2</sub> (1:1) mixture at much lower pressure (~10<sup>-3</sup> mbar) and mainly proceed along the step edges. The results indicate that the structural

stability of the Au/ceria catalysts is intimately connected with its reactivity in the CO oxidation reaction. The results show both similarities and differences with the previously studied Au/TiO<sub>2</sub>(110) and Au/FeO(111) systems, which implies that Au/oxide interaction is directly involved in the structural stability of the supported gold catalysts.

#### Acknowledgments

The authors gratefully acknowledge financial support from the Fonds der Chemischen Industrie and Deutsche Forschungsgemeinschaft (DFG). J.L. thanks International Max-Planck Research School “Complex Surfaces in Materials Science” for the fellowship.

#### References

- [1] G. Bond, C. Lois and D. Thompson, *Catalysis by Gold* (World Scientific, 2006).
- [2] Q. Fu, A. Weber and M. Flytzani-Stephanopoulos, *Catal. Lett.* 77 (2001) 87.
- [3] D. Andreeva, V. Idakiev, T. Tabakova, L. Ilieva, P. Falares A. Bourlinos and A. Travlos, *Catal. Today* 72 (2002) 51.
- [4] H. Sakurai, T. Akita, S. Tsubota, M. Kiuchi and M. Haruta, *Appl. Catal. A* 291 (2005) 179.
- [5] S. Carrettin, P. Concepción, A. Corma, J.M. López Nieto and V.F. Puntes, *Angew. Chem. Int. Ed.* 43 (2004) 2538.
- [6] J. Guzman, S. Carrettin and A. Corma, *J. Am. Chem. Soc.* 127 (2005) 3286.
- [7] S.-Y. Lai, Y. Qiu and S. Wang, *J. Catal.* 237 (2006) 303.
- [8] M.A. Centeno, C. Portales, I. Carrizosa and J.A. Odrizola, *Catal. Lett.* 102 (2005) 289.
- [9] U.R. Pillai and S. Deevi, *Appl. Catal. A* 299 (2006) 266.
- [10] Q. Fu, H. Saltsburg and M. Flytzani-Stephanopoulos, *Science* 301 (2003) 935.
- [11] C.T. Campbell, *Surf. Sci. Rep.* 27 (1997) 1.
- [12] C. Henry, *Surf. Sci. Rep.* 31 (1998) 231.
- [13] D.W. Goodman, *Chem. Rev.* 95 (1995) 523.
- [14] H.-J. Freund, *Surf. Sci.* 500 (2002) 271.



- [15] R. Meyer, C. Lemire, S. Shaikhutdinov and H.-J. Freund, *Gold Bull.* 37 (2004) 72.
- [16] J. Guzman and B.C. Gates, *J. Am. Chem. Soc.* 126 (2004) 2672; *J. Phys. Chem. B* 106 (2002) 7659.
- [17] J.D. Henao, T. Caputo, J.H. Yang, M.C. Kung and H.H. Kung, *J. Phys. Chem. B* 110 (2006) 8689.
- [18] X. Wang, J.A. Rodriguez, J.C. Hanson, M. Perez and J. Evans, *J. Chem. Phys.* 1213 (2005) 21101.
- [19] S.H. Overbury, V. Schwartz, D. Mullins, W. Yan and S. Dai, *J. Catal.* 241 (2006) 56.
- [20] N. Weiher, *J. Catal.* 240 (2006) 100.
- [21] G. Hutchings, *J. Catal.* 242 (2006) 71.
- [22] M. Valden, X. Lai and D.W. Goodman, *Science* 281 (1998) 1647.
- [23] A. Kolmakov and D.W. Goodman, *Catal. Lett.* 70 (2000) 93.
- [24] D.E. Starr, S.K. Shaikhutdinov and H.-J. Freund, *Top. Catal.* 36 (2005) 33.
- [25] D.R. Mullins, P.V. Radulovic and S.H. Overbury, *Surf. Sci.* 429 (1999) 186.
- [26] J.-L. Lu, H.-J. Gao, S. Shaikhutdinov and H.-J. Freund, *Surf. Sci.* (corrected proof available online).
- [27] H. Nörenberg and G.A.D. Briggs, *Surf. Sci.* 424 (1999) L352.
- [28] S. Eck, C. Castellarin-Cudia, S. Surnev, M.G. Ramsey and F.P. Netzer, *Surf. Sci.* 520 (2002) 173.
- [29] C. Castellarin-Cudia, S. Surnev, G. Schneider, R. Podlucky, M.G. Ramsey and F.P. Netzer, *Surf. Sci.* 554 (2004) L120.
- [30] F. Esch, S. Fabris, L. Zhou, T. Montini, C. Africh, P. Fornasiero, G. Comelli and R. Rosei, *Science* 309 (2005) 752.
- [31] T. Akita, M. Okumura, K. Tanaka, M. Kohyama, S. Tsubota and M. Haruta, *J. Electron Microsc.* 54 (2005) 81; *J. Mat. Sci.* 40 (2005) 3101.
- [32] T.X.T. Sayle, S.C. Parker and C.R.A. Catlow, *Surf. Sci.* 316 (1994) 329.